JMEPEG (2011) 20:762–766
DOI: 10.1007/s11665-010-9817-8
©ASM International
1059-9495/$19.00

Effects of Sn and Zr on the Microstructure and Mechanical Properties of Ti-Ta-Based Shape Memory Alloys

Y.X. Tong, B. Guo, Y.F. Zheng, C.Y. Chung, and L.W. Ma

(Submitted May 16, 2010; in revised form September 29, 2010)

Ti-Ta binary shape memory alloys have attracted much interest due to the absence of toxic element and the low Young's modulus. However, the effects of the third element on the microstructure and mechanical property had not been well understood. In the present study, the effect of Sn and Zr additions on the microstructure and mechanical property of Ti-35Ta (at.%) alloys has been investigated. The results show that the microstructure of the solution treated Ti-Ta-based alloys compose of equiaxial grains. The alloys consist of β-phase and α″ martensite phase at room temperature, except for the Ti-30Ta-5Sn alloy which consists of only β-phase. This is possibly due to the presence of Sn which provides a stronger β-stabilized effect on quenching compared to Zr addition. The lattice parameter of the β-phase increased with the increase in Sn and Zr content. The addition of Sn and Zr had caused obvious increase in the tensile strength. The corrosion resistance of Ti-Ta-based alloys was also improved by adding Sn.

Keywords mechanical property, microstructure, shape memory alloy, Ti-Ta

1. Introduction

Titanium alloys are widely used for dental implants and orthodontic surgery applications. Although titanium and the popular Ti-6Al-4V alloys have excellent reputation for their high strength, low density (high specific strength), high immunity to corrosion and biocompatibility, the long-term performance of these alloys has raised some concerns due to the possible release of elements aluminum and vanadium which were found associated with health problems, such as Alzheimer disease, neuropathy, and allergic reaction (Ref 1-3). Another issue concerned is the mismatch between high modulus of metallic implants and low modulus of bone causing biomechanical incompatibility known as "stress shielding" problem (Ref 4). In the past decades, Nb, Ta, Zr, and Sn have been considered excellent β-stabilizing alloying elements for titanium alloys (Ref 5), which are also biocompatible. Therefore, β-type titanium alloys, such as Ti-35.5Nb-5Ta-7Zr (Ref 6, 7), Ti-29Nb-13Ta-4.6Zr (Ref 8-10), and Ti-24Nb-4Zr-7.9Sn (Ref 11, 12), have been developed as biomedical shape memory and superelastic alloys.

Among these candidates, Ti-Ta binary alloys have attracted great interest due to its good combination of high strength, low modulus, as well as potential good shape memory alloy properties (Ref 13, 14). The corrosion resistance of Ti-Ta alloys is superior to that of pure Ti, which increases with increase in Ta content (Ref 15). The effects of ternary alloying elements on phase constitution, aging behavior, and shape memory behavior of Ti-Ta binary alloys has been investigated (Ref 16-18). The decrease in the martensitic transformation temperature due to Zr, Hf, Sn alloying in Ti-30Ta-*X* (at.%) was affected by larger number of valence electrons and smaller atomic radius of the alloying elements. The addition of Sn to Ti-Ta was found suppressing the effect of aging on shape memory behavior due to the ω-phase formation (Ref 17). The substitution of Zr for Ta can improve the shape memory effect of Ti-50Ta alloy (Ref 18).

However, the effect of third element on the microstructure, mechanical property, and corrosion behavior of Ti-Ta binary alloys has not been reported. The aim of the present study is to investigate the effects of Sn and Zr additions on the microstructure, mechanical property, and corrosion behavior of Ti-35Ta (at.%) alloys.

2. Experimental Procedures

Ti-$(35 - x)$Ta-xSn and Ti-$(35 - x)$Ta-xZr (x = 0, 1, 5, all in at.%) alloys were prepared using arc melting furnace with water-cooled copper hearth under a high purity argon atmosphere from Ti wire (99.8%), Ta wire (99.9%), Zr wire (99.9%), and Sn sheet (99.9%) as raw materials. Owing to the big differences in melting point (Ti: 1953 K; Ta: 3273 K) and density (Ti: 4.51 g/cm^3; Ta: 16.6 g/cm^3) between pure Ti and

This article is an invited paper selected from presentations at Shape Memory and Superelastic Technologies 2010, held May 16-20, 2010, in Pacific Grove, California, and has been expanded from the original presentation.

Y.X. Tong, B. Guo, and **Y.F. Zheng**, Center for Biomedical Materials and Engineering, Harbin Engineering University, Harbin 150001, China; and **C.Y. Chung** and **L.W. Ma**, Department of Physics and Materials Science, City University of Hong Kong, 83 Tat Chee Avenue, Kowloon Tong, Hong Kong. Contact e-mail: appchung@cityu.edu.hk.

pure Ta, the ingots were re-melted for 10 times, and flipped over after each melting to achieve chemical homogeneity. The button-shaped ingots were hot rolled 90% into approximately 1-mm thick plates at 1173 K, then solution treated at 1173 K for 3.6 ks and quenched into water.

The microstructure was studied by optical microscope, after the samples were ground, polished, and etched in a solution composed of HF, HNO_3, and water (1:1:8 in volume). Phase constitution at room temperature was determined by x-ray diffraction (XRD), using Cu Kα radiation in the typical range of $2\theta = 20°$ to 100° at an accelerating voltage of 40 kV, a current of 40 mA, and a scanning speed of 2°/min.

Mechanical behavior was characterized by tensile test at a strain rate of 8.33×10^{-5}/s at room temperature. The samples used for tensile tests were rectangular shaped with a gage length of 20 mm and a cross section of 2 mm (width) × 1 mm (thickness). The fracture surface was examined by scanning electron microscope (SEM).

The samples prepared for electrochemical measurements were cut from the solution-treated samples with a dimension of $1 \times 1 \times 0.1$ cm^3. After mechanically polished with water-proof silicon carbide paper up to 2000# grid, all the samples were cleaned with acetone, ethanol and de-ionized water in an ultrasonic bath. These samples were dried by hot air. The sample, a platinum electrode and a saturated calomel electrode (SCE) were used as working electrode, counter electrode and reference electrode, respectively. The electrolyte used to simulate human body corrosion condition was Hank's solution prepared using de-ionized water. The chemical composition of the Hank's solution is 8 g/L NaCl, 0.14 g/L $CaCl_2$, 0.4 g/L KCl, 0.1 g/L $MgCl_2 \cdot 6H_2O$, 0.06 g/L $MgSO_4 \cdot 7H_2O$, 0.35 g/L $NaHCO_3$, 0.06 g/L KH_2PO_4, 0.06 g/L $Na_2HPO_4 \cdot 2H_2O$, 1 g/L glucose (Ref 19). The pH values of the solution were maintained at 7.4 by adding HCl or NaOH. The potential dynamic polarization curves were conducted from −0.8 V (vs. SCE) to 2.0 V (vs. SCE) with a scan rate of 1 mV/s after 3.6 ks immersion.

3. Experimental Results

Figure 1 shows the optical microscopic images of Ti-Ta-based alloys. It is seen that the microstructure is characterized by equiaxial grain. The small dark spots in Fig. 1 are possibly dislocation etch pits, which are often observed in the metallographic of heavy deformed Ti alloy. The average grain size of Ti-35Ta is about 15 μm shown in Fig. 1(a). The grain size becomes slightly larger with the additions of Sn and Zr, and the grain boundary becomes wider for Ti-Ta-Sn alloys, as shown in Fig. 1(b) and (c). This implies a higher etching rate at the grain boundaries relative to the grain matrix.

It can be found from Fig. 2(a) that Ti-35Ta alloy consists of a mixture of β-phase with a BCC structure and α″ martensite phase with an orthorhombic structure. With increase in Sn content, the diffraction peak corresponding to α″ martensite gradually becomes weaker, and finally disappear. The addition of Zr does not significantly affect the phase constitution of Ti-Ta alloys. This implies that the addition of Sn may provide a stronger β-stabilized effect on quenching compared to that of Zr. This agrees well with the previous results on Ti-30Ta (at.%) alloys (Ref 17). Figure 2(b) shows the dependence of lattice parameter of β-phase on the content

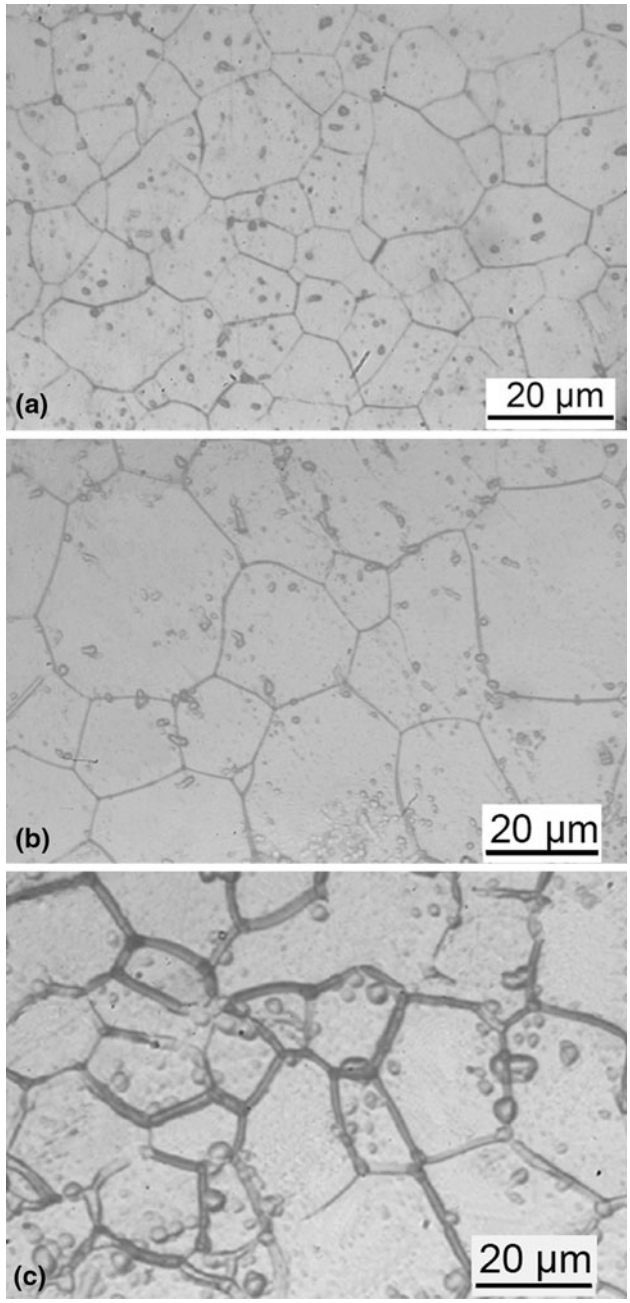

Fig. 1 Optical microstructure of Ti-35Ta (a), Ti-30Ta-5Zr (b), and Ti-30Ta-5Sn alloys (c)

of the third elements. The lattice parameter increases obviously with increase in Sn (5%), whereas it increases only insignificantly with the addition of Zr.

Figure 3(a) shows the stress-strain curves for Ti-Ta-based alloys. Ti-35Ta exhibits a "double yielding" phenomenon, in which the first "yielding" corresponds to rearrangement of martensite variant and the stress-induced martensite (SIM) transformation from β to α″, indicated by blank-headed arrows, the second "yielding" corresponds to plastic deformation of α″ martensite labeled with black-headed arrows. The critical yield stress for SIM increases with the addition of Sn and Zr. Ti-30Ta-5Sn exhibits "single yielding" due to its lower critical stress level for plastic deformation than critical

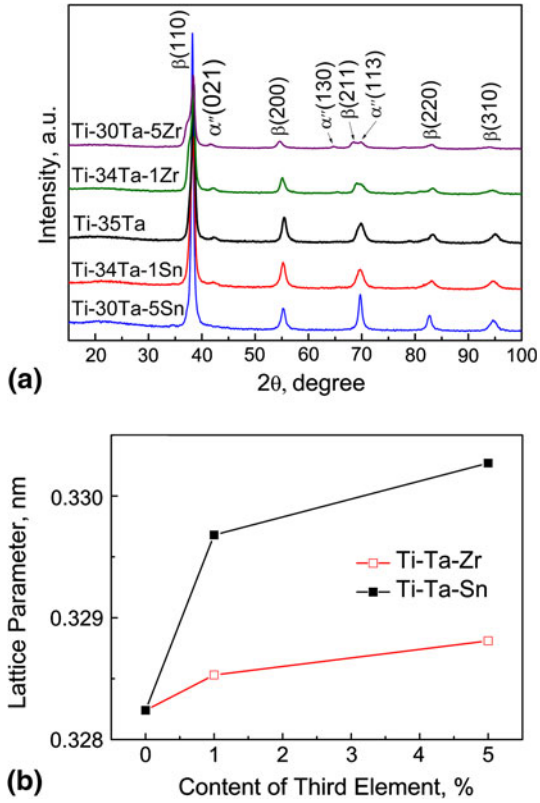

Fig. 2 XRD patterns of Ti-Ta-based alloys (a), effect of third element content on lattice parameter of β-phase in Ti-Ta-based alloys (b)

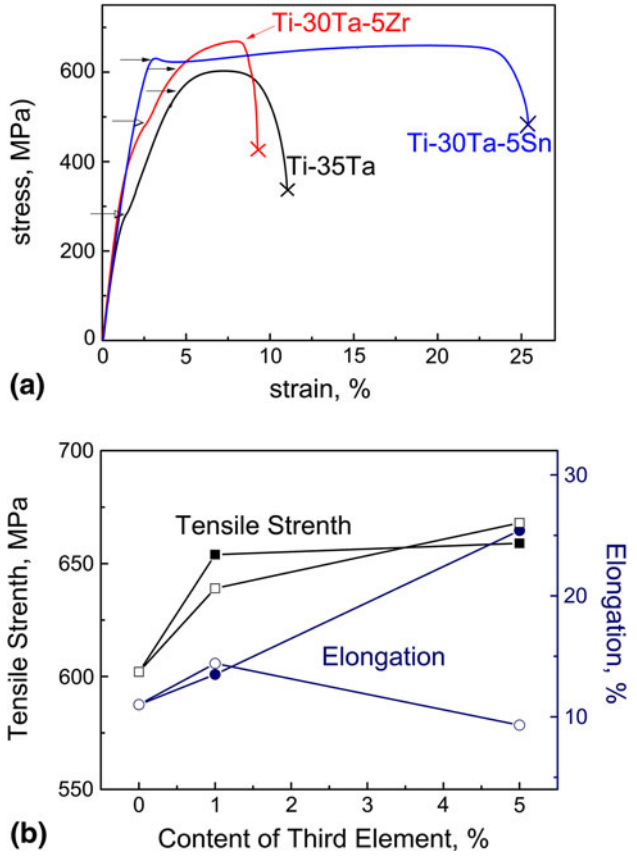

Fig. 3 Stress-strain curves of Ti-Ta-based alloys (a), effect of third element on tensile strength and elongation to fracture of Ti-Ta-based alloys (solid symbols represent Ti-Ta-Sn alloys, open symbols Ti-Ta-Zr alloys) (b)

stress for SIM. This implies that parent β-phase becomes stable at room temperature and martensite transformation start temperature (*M*s) decreases with Sn and Zr content increasing. In contrast, Sn is more effective in stabilizing the β-phase, lowering the *M*s and raising the critical stress for SIM compared to Zr. These results are consistent with the XRD results shown in Fig. 2.

Mechanical properties, including tensile strength and elongation to fracture were evaluated by plotting the tensile strength against Sn and Zr content, as shown in Fig. 3(b). It can be found that the tensile strength of Ti-Ta-based alloys increases with the additions of Sn and Zr. The elongation to fracture also increases with increase in Sn content monotonously. On the other hand, the elongation increases with increase in Zr content and reaches the maximum at 1%. Subsequently, it decreases on further increase of Zr content to 5%.

The SEM images of the fracture surface morphologies of Ti-Ta-based alloys after tensile tests are shown in Fig. 4(a-c). Ti-35Ta alloy exhibits typical ductile fracture with dimple patterns, as seen in Fig. 4(a). Although the fracture surface of Ti-30Ta-5Zr also composed of dimple patterns, a few cleavage planes can also be observed as shown in Fig. 4(b), indicating a decrease in ductility with Zr addition. On the contrary, the fracture morphologies of dimple patterns are more homogeneous for Ti-30Ta-5Sn alloy than that of Ti-35Ta, as shown in Fig. 4(c), which infers a better plasticity with Sn addition.

Figure 5 shows the potential dynamic polarization curves of Ti-Ta-based alloys after immersion in Hank's solution for 3.6 ks. All of the studied alloys exhibit wide passive region, which means that the passive films formed on the surface of samples are protective, thus preventing further corrosion. It is interesting to note that Ti-35Ta and Ti-30Ta-5Sn alloys show clear active-passive transition, in contrast to Ti-30Ta-5Zr without showing obvious active-passive transition. The corrosion current densities (I_{corr}) were estimated by Tafel analysis using both cathodic and anodic branches of the polarization curves. It is evident that Ti-30Ta-5Sn exhibits reduced I_{corr}, while Ti-30Ta-5Zr exhibits increased I_{corr}. The passivation current density (I_{pass}) as determined at 0.5 V is approximately 10.1 μA/cm^2 for Ti-35Ta, and 9.67 μA/cm^2 for Ti-30Ta-5Sn. On the contrary, the I_{pass} at 0.5 V increases to 30.4 μA/cm^2 for Ti-30Ta-5Zr. The lower I_{corr} and I_{pass} with Sn element addition indicates an improved corrosion resistance compared to the Ti-35Ta binary alloy, while the higher I_{pass} and I_{corr} with Zr element addition indicates a poorer corrosion resistance compared to the Ti-35Ta alloy.

4. Conclusions

The alloys consist of β-phase and α″ martensite phase at room temperature except for Ti-30Ta-5Sn which consists of only β-phase. The Sn element provides a stronger β-stabilized

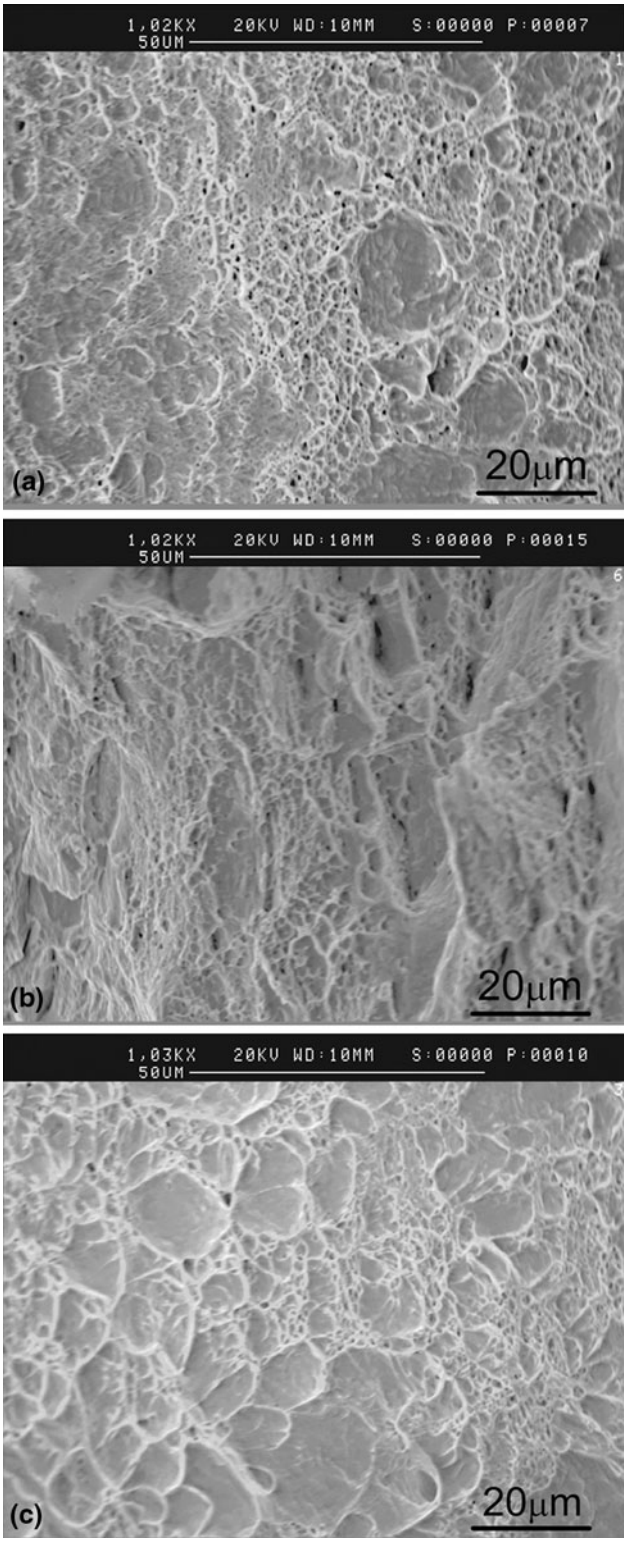

Fig. 4 SEM image of fracture surface of Ti-35Ta (a), Ti-30Ta-5Zr (b), and Ti-30Ta-5Sn alloy (c)

effect on quenching relative to Zr addition. The lattice parameter of β-phase increase with the increasing of Sn and Zr content. The tensile strength were also improved. The elongation to fracture increases with the content of Sn increased. The corrosion resistance is improved by Sn addition.

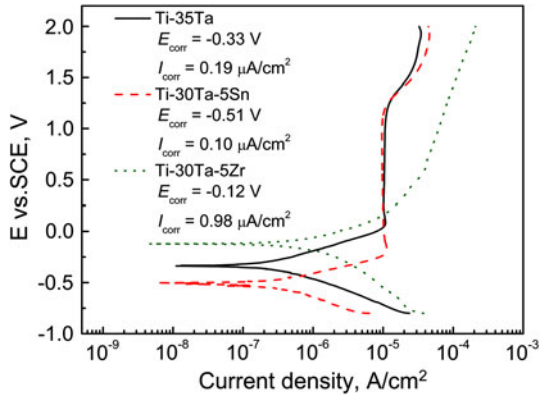

Fig. 5 The potential dynamic polarization curves of Ti-Ta-based alloys in Hank's solution

Acknowledgment

The work was supported by a grant from the Research Grant Council of the City University of Hong Kong, China (CityU SRG project #7002215). This work was also supported by the Fundamental Research Funds for the Central Universities (HEU-CF101013).

References

1. M. Geetha, A.K. Singh, R. Asokamani, R. Asokamani, and A.K. Gogia, Ti Based Biomaterials, the Ultimate Choice for Orthopaedic Implants—A Review, *Prog. Mater. Sci.*, 2009, **54**(3), p 397–425
2. B. Platt, G. Fiddler, G. Riedel, and Z. Henderson, Aluminium Toxicity in the Rat Brain: Histochemical and Immunocytochemical Evidence, *Brain Res. Bull.*, 2001, **55**(2), p 257–267
3. S. Rao, T. Ushida, T. Tateishi, Y. Okazaki, and S. Asao, Effect of Ti, Al, and V Ions on the Relative Growth Rate of Fibroblasts (L929) and Osteoblasts (MC3T3-E1) Cells, *Bio-Med. Mater. Eng.*, 1996, **6**(2), p 79–86
4. D.R. Sumner, T.M. Turner, R. Igloria, R.M. Urban, and J.O. Galante, Functional Adaptation and Ingrowth of Bone Vary as a Function of Hip Implant Stiffness, *J. Biomech.*, 1998, **31**(10), p 909–917
5. E. Eisenbarth, D. Velten, M. Müller, R. Thull, and J. Breme, Biocompatibility of [Beta]-Stabilizing Elements of Titanium Alloys, *Biomaterials*, 2004, **25**(26), p 5705–5713
6. M. Long, R. Crooks, and H.J. Rack, High-Cycle Fatigue Performance of Solution-Treated Metastable-[Beta] Titanium Alloys, *Acta Mater.*, 1999, **47**(2), p 661–669
7. R. Banerjee, S. Nag, and H.L. Fraser, A Novel Combinatorial Approach to the Development of Beta Titanium Alloys for Orthopaedic Implants, *Mater. Sci. Eng. C*, 2005, **25**(3), p 282–289
8. D. Kuroda, M. Niinomi, M. Morinaga, Y. Kato, and T. Yashiro, Design and Mechanical Properties of New β Type Titanium Alloys for Implant Materials, *Mater. Sci. Eng. A*, 1998, **243**(1–2), p 244–249
9. M. Niinomi, D. Kuroda, K. Fukunaga, M. Morinaga, Y. Kato, T. Yashiro, and A. Suzuki, Corrosion Wear Fracture of New β Type Biomedical Titanium Alloys, *Mater. Sci. Eng. A*, 1999, **263**(2), p 193–199
10. M. Niinomi, Fatigue Performance and Cyto-toxicity of Low Rigidity Titanium Alloy, Ti-29Nb-13Ta-4.6Zr, *Biomaterials*, 2003, **24**(16), p 2673–2683
11. Y.L. Hao, S.J. Li, S.Y. Sun, C.Y. Zheng, and R. Yang, Elastic Deformation Behaviour of Ti-24Nb-4Zr-7.9Sn for Biomedical Applications, *Acta Biomater.*, 2007, **3**(2), p 277–286
12. S.J. Li, T.C. Cui, Y.L. Hao, and R. Yang, Fatigue Properties of a Metastable [Beta]-Type Titanium Alloy with Reversible Phase Transformation, *Acta Biomater.*, 2008, **4**(2), p 305–317
13. Y.L. Zhou, M. Niinomi, and T. Akahori, Effects of Ta Content on Young's Modulus and Tensile Properties of Binary Ti-Ta Alloys for

Biomedical Applications, *Mater. Sci. Eng. A*, 2004, **371**(1–2), p 283–290
14. P.J.S. Buenconsejo, H.Y. Kim, H. Hosoda, and S. Miyazaki, Shape Memory Behavior of Ti-Ta and its Potential as a High-Temperature Shape Memory Alloy, *Acta Mater.*, 2009, **57**(4), p 1068–1077
15. K.A. de Souza and A. Robin, Preparation and Characterization of Ti-Ta Alloys for Application in Corrosive Media, *Mater. Lett.*, 2003, **57**(20), p 3010–3016
16. M. Ikeda, S.Y. Komatsu, and Y. Nakamura, Effects of Sn and Zr Additions on Phase Constitution and Aging Behavior of Ti-50mass% Ta Alloys Quenched from β Single Phase Region, *Mater. Trans.*, 2004, **45**(4), p 1106–1112
17. P.J.S. Buenconsejo, H.Y. Kim, and S. Miyazaki, Effect of Ternary Alloying Elements on the Shape Memory Behavior of Ti-Ta Alloys, *Acta Mater.*, 2009, **57**(8), p 2509–2515
18. T. Peradze, I. Stamateli, J. Cederstrom, T. Berikashvili, A. Razov, and K. Gorgadze, Shape Memory Effect in Ti-Ta-Zr Alloys, *Int. J. Appl. Electromagn. Mech.*, 2006, **23**(1–2), p 39–43
19. Y.F. Zheng, B.L. Wang, J.G. Wang, C. Li, and L.C. Zhao, Corrosion Behaviour of Ti-Nb-Sn Shape Memory Alloys in Different Simulated Body Solutions, *Mater. Sci. Eng. A*, 2004, **338–440**, p 891–895